Received: 21 April 2021 | Accepted: 21 April 2021

DOI: 10.1002/cend.202100015

FULL PAPER

Ernst & Sohn
A Wiley Brand

Ground motions induced by wind turbines

Sven Nagel[1] | Toni Zieger[2] | Birger Luhmann[3] | Peter Knödel[1] | Joachim Ritter[2] | Thomas Ummenhofer[1]

[1]Karlsruher Institut für Technologie, Stahl- und Leichtbau, Karlsruhe, Germany

[2]Formerly at Geophysikalisches Institut, Karlsruher Institut für Technologie, Karlsruhe, Germany

[3]Stuttgarter Lehrstuhl für Windenergie, Institut für Flugzeugbau, Universität Stuttgart, Stuttgart-Vaihingen, Germany

Correspondence
Sven Nagel, Karlsruher Institut für Technologie, Stahl- und Leichtbau, Otto-Ammann-Platz 1, 76131 Karlsruhe, Germany.
Email: nagel.sven@gmail.com

Abstract

Wind flow transfers forces to the wind turbine's rotor blades. These then set the rotor in motion. The hub and the gearbox, where present, transfer this rotational energy to the generator for conversion into electrical power. All the rotating components have significant mass and are located at the head of a slender, elastic load-bearing tower in which they induce dynamic effects. The resulting vibrations, generated at the upper end of the tower, are modified by the dynamic properties of the tower structure and pass through the foundations into the ground. Broadband seismometers record these ground vibrations not only directly adjacent to the wind turbine but also at greater distances of (up to) several kilometers from the turbine. We are aware that local residents and opponents of wind power consider that these vibration phenomena bear potential negative health effects. In the context of this paper, seismic vibrations were measured at the foundation of a 2 MW reference turbine. These seismic signals were compared to numerical simulations. Based on this, we explain the physical background. In the past, any ground vibrations measured have usually been attributed exclusively to the excitation frequencies from the rotor. However, the investigations presented here show that the structural properties of the tower structure significantly influence the type and intensity of the vibrations induced in the ground and dominate the ground motion amplitudes. Finally, we show that the targeted use of absorbers can significantly reduce the vibrations induced in the ground.

KEYWORDS
hybrid tower, multi-body simulation, seismology, vibration, wind energy

1 | WIND TURBINES ARE COMPLEX, DYNAMIC SYSTEMS

1.1 | Terms and abbreviations

WT	Wind turbine
Seismic vibrations	Vibrations comprising one or more wavelengths which propagate through the ground
TBEF	Natural tower bending frequency
Ω	Angular frequency of the rotor speed
1P-excitation	Excitation of the WT at a frequency which corresponds to the rotational speed Ω (See Section 3.3 for details).
3P-excitation	Excitation of the WT at the rotor blade transient frequency $n \cdot \Omega$, where n is the number of rotor blades; usually $n = 3$; the term 3P excitation has been established for this (See Section 3.3 for details).
Power density/power density spectrum	This is used here as a reference value to assess the power induced in the ground. More generally, a power density spectrum corresponds to the power

(Continues)

The paper was initially published in German: Nagel, S., Zieger, T., Luhmann, B., Knödel, P., Ritter, J. and Ummenhofer, T. (2019), Erschütterungsemissionen von Windenergieanlagen. Stahlbau, 88: 559-573. https://doi.org/10.1002/stab.201900039.

	contained in the seismic time signal over a defined period as a function of the frequency contained in the signal; the calculation is performed on the basis of the kinetic energy ($W_{kin} = 0.5 \cdot m \cdot v^2$) from the square of the ground motion velocity (or suitable alternative values for comparison purposes)
Ocean microseisms	Movements of the Earth measurable inland at frequencies ≤0.2 Hz which are caused by the ocean waves.
DLC	Design load cases—measurement scenarios after[1] which describe a WT's operating and emergency states.

2 | INTRODUCTION

In terms of steel wind turbines (WT), factors playing a key role in design are: the large number of cycles which are relevant to fatigue; the stability behavior of the tubular tower, and connections.[2–5] Besides these constraints directly affecting measurement of the load-bearing structure, cyclical excitation by the rotor also causes many further dynamic phenomena in the area surrounding the WT. The heated debate about thresholds for vibration and the disruptive influences uncovered during seismic measurements motivated the authors to undertake the present study.

The authors aimed to identify the sources of sound and vibration in a WT, investigate the propagation of dynamic excitation, and demonstrate any potential for reducing the vibrations emitted.

The investigations under discussion here formed part of the umbrella project TremAc. This is supported by the Federal German Ministry for Economic Affairs and Energy, on the basis of a decision made by the Bundestag.[6] It aims to draw up objective criteria by which to assess vibration and sound emissions from onshore WTs. This involves identifying the main parameters needed for an objective assessment of turbine sound and vibration emissions. The sources and transmission routes for sound in air and vibrations in the ground are identified and investigated using numerical simulation (finite element analysis, computational fluid dynamics, boundary element method, multi-body simulation [MBS]) and measurements. Accompanying environmental health and environmental psychology investigations aim to provide an objective basis for the health risks expected to result from WTs. The present paper discusses investigations into the background for the vibration phenomena occurring in the area around WT foundations. The main focus for investigation in the TremAc project as a whole is shown in Figure 1 and presented in a wider context in Reference 7. Numerical studies on the propagation of sound and seismic vibrations are conducted by the Institute of Soil Mechanics and Rock Mechanics (IBF) and the Geophysical Institute (GPI) at the Karlsruhe Institute of Technology (KIT) and described in Reference 8. A detailed linked flow simulation using flexible tower and blade structures is being conducted at the Institute of Aerodynamics and Gas Dynamics (IAG) at the University of Stuttgart.[9]

2.1 | Sample turbine and generic simulation model

The research described below relates to a common 2 MW WT; the type and location have been anonymized. The turbine has a hub height of ~140 m. The combined mass of the rotor blades, nacelle and generator is ~150 t. According to the information plate affixed to the WT, the supporting structure is a hybrid tower[10] with a mass of ~1650 t. The bottom 90 m of the tower structure is built from 24 precast reinforced steel elements that are pretensioned against each other; the top third consists of a tubular steel tower. Market analysis which KIT performed based on the Register of Assets held by the Bundesnetzagentur (Federal German Network Agency for Electricity, Gas, Telecommunications, Post and Railway)[11] shows that this combination of two materials is the most common construction method for towers of > 120 m built in Germany between September 2014 and July 2016 (work package C2 in Reference 6). The reason for this is the diameter required at the base of the tower to provide the necessary rigidity. At hub heights of > 80 m this diameter normally exceeds 4 m, thus making it difficult or practically impossible to transport premanufactured tubular steel sections. The alternative to tubular steel is precast concrete segments only a few meters high, several of which would make up the circumference of the tower. In addition to hybrid towers, alternative steel designs are increasingly being used. These include chamfered segments bolted together lengthways,[12] which have also been investigated numerically as part of the TremAc study.

The turbine we investigated has flat circular reinforced concrete foundations with a diameter of ~20 m, embedded to a depth of ~3.5 m. Its operating range starts at a mean wind speed of 2.5 m/s and covers rotation speeds of 6 to 19.5 rpm.

We derived a generic MBS model from these macroparameters (Section 4.5). This includes the blade geometry in order to determine the flow forces which depend on the incident flow speed, as well as a control system and all structural components. The model is based on a generic WT developed at the Technical University of Munich Wind Energy Institute.[13] This was scaled and modified for the actual rated output and geometry using an integrated optimization algorithm. The control system was modified at Stuttgart Wind Energy (Germany's first university chair for wind energy) to reflect the main characteristics of the reference turbine. The generic tower structure was modified using publicly available data so that the overall model has comparable geometric and structural dynamic properties to the real WT. Static stress capacity and dynamic properties were also specifically added to the settings. We did not conduct individual investigations to find evidence of fatigue because the task at hand only required a plausible overall model for dynamic properties.

The rigidity of the foundations and the dynamic ground properties we applied were based on research by the IBF at the KIT and

were depicted using analytical half-space approaches as frequency-dependent translational and rotational degrees of freedom. The foundations pass through a layer of sand and tie into limestone. For the purposes of the present study, stratification has not been considered and instead the reference values for limestone have been used for calculations (density $\rho \approx 2600$ kg/m^3, shear modulus $G \approx 1.25e + 10$ N/m^2, shear wave velocity $c_s = 2150$ -2200 m/s).

These effects must be considered when calculating the propagation of vibrations. As we are primarily focusing on low frequency excitations, these effects will be considered as the mean values in the calculation models, regardless of frequency.[14]

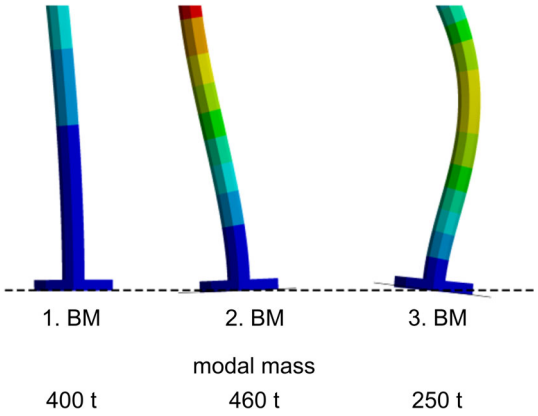

FIGURE 1 The main topics researched by the TremAc project

3 | VIBRATION PHENOMENA IN WTs

3.1 | The principles of dynamic tower structure design

The dynamic design of the whole turbine exerts a major influence on load-bearing and fatigue-related safety analyses. Cases of resonance where the structure's natural frequencies match the rotor excitation must be avoided throughout the operating area. This can be achieved by specifically coordinating the stiffness and weight ratios of the tower structure and head weight (ie, nacelle, blades, generator and gearbox). Similar action is recommended for all other turbine components susceptible to vibration. The resonance diagrams shown in Figure 2 explain the background to this (Campbell diagrams).[15] These diagrams plot the natural frequencies and excitation frequencies against the rotor speed. The solid vertical lines (cut-in speed and rated speed) mark out the operating range of common variable-speed turbines. The dashed horizontal lines show the natural frequencies for the structure as a whole (tower and head weight), which do not depend on speed. It should be ensured that these natural frequencies do not intersect within the operating range with one of the speed-dependent rotor excitations (1P and 3P frequencies). Different coordination strategies will be applied according to tower design and hub height.

As discussed in References 15 and 16 smaller WTs have in the past been designed using a “stiff-stiff” approach as shown in Figure 2 (on the left). In this case the tower is so stiff that the natural frequencies for the entire system lie above both dominant excitation

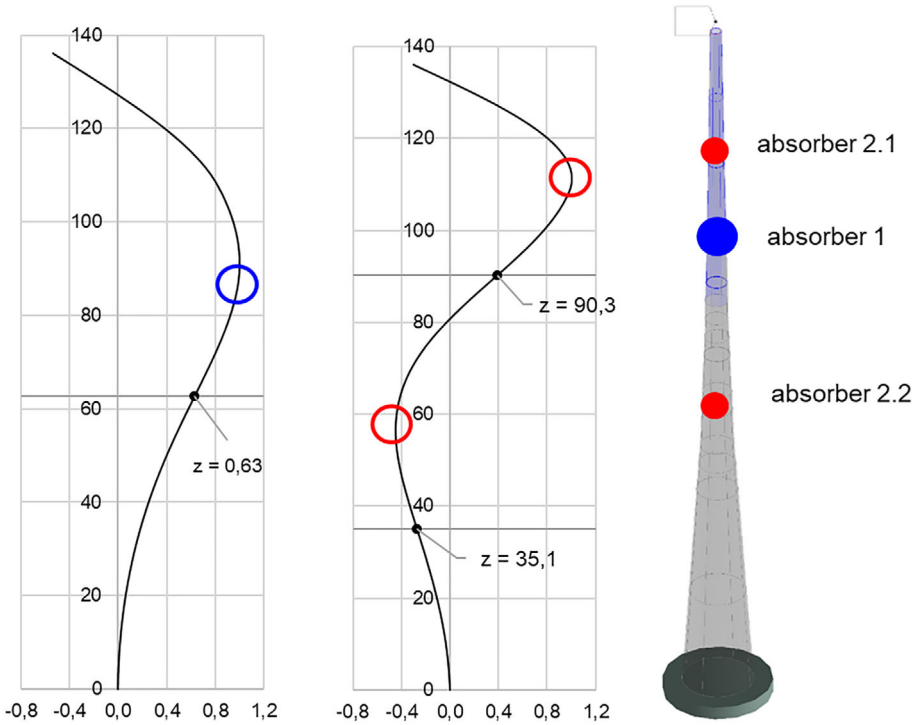

FIGURE 2 Campbell diagram for the dynamic design of a wind turbine; left: stiff-stiff, middle: soft-stiff, right: soft-soft

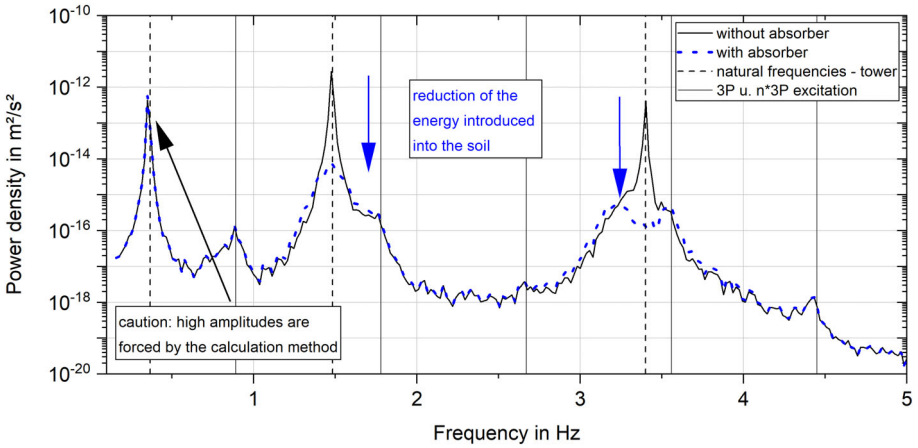

FIGURE 3 The effect of mass imbalances in the rotor of a WT

frequencies (1P and 3P). The natural frequency for a single mass oscillator is determined by the ratio of stiffness to mass using the square root, so that a doubling in stiffness when mass remains the same increases the natural frequency by a factor of 1.41.[16]

For larger WTs this is not economically viable, which means that their tower structures are normally built according to the "soft-stiff" principle. Figure 2 shows this combination (in the middle). The first natural system frequency lies within the operating range, below the 3P (soft) but above the 1P frequency (stiff). Every time the WT begins to operate, the system must pass through the points of resonance (marked with a circle) for both 3P excitation and the first natural frequency. Compared to a single mass oscillator undergoing harmonic force excitation, this means subcritical operation with regard to the 1P excitation and supercritical operation with regard to the 3P excitation. The amplification functions explained in Reference 17 show that, given an appropriate design, the dynamic loads arising in the supercritical state can be lower than the statically relevant stress; this also allows for additional savings in materials. Figure 2 (on the right) outlines the "soft-soft" design identified in Reference 16 as especially economical for large turbines, although in practice such WTs remain rare.With this design, the tower's construction is so soft that the first system natural frequency within the operating range lies below both the 3P and 1P excitations.

The greater deformation of the whole turbine which accompanies a soft design can, for example, mean that the aerodynamic attenuation described in Section 3.4 plays a greater role in dynamic balancing. Lange and Elberg[16] discuss further advantages and disadvantages of a soft design and assess these against load spectra. With a real WT, normative rules[1,18] such as variations in the natural frequencies or in the speed which need to be considered, are used alongside the above design principles.

3.2 | Types of load

Besides quasi-static loads, for example, from dead weight or mean rotor thrust arising from mean wind speed, temporal variations in load have different characteristic effects on the load-bearing structure. Periodic excitation correlating to the rotational speed and its multiples determines the dynamic design of all the components in a WT in the operating state.

The causes of some major types of excitation are discussed below and form the heart of the present research. Even where the rotor is stationary, a Kármán vortex[17] can cause periodic excitation of the tubular WT tower at right angles to the incident flow, for example, due to interaction between the tubular tower and the flow. The periodic effects and the associated stress range which impacts on fatigue come into play in many cases when dimensioning WT components. For example, over a projected 20-year lifetime or operation, figures for load cycles on the rotor axle may be in the order of 10^{9}[19] load cycles, calling into question established fatigue concepts. However, findings currently referred to by the terms giga-cycle fatigue or ultra-high-cycle fatigue[20–22] do not form the basis for the lack of durability in the S-N curves from Reference 18. Erratic gusts in the turbulent wind field lead to further stochastic, transient time signals. The present paper records these in the numerical simulation of operating conditions. For example, they cause variations in rotational speed and therefore a lack of clarity in the results. Pulse loads arising from the turbine control or an emergency shutdown lie outside the scope of our investigation.

3.3 | Describing selected excitation phenomena

The typical excitation of a WT arises in line with the rotor speed Ω and its multiples. These excitations can be ascribed to various sets of causes. For example, we will present typical examples to represent the "rotating mass" and "aerodynamic excitation" sets. These are intended to give an impression of how diverse vibration phenomena are and enable the reader to follow our subsequent assessments.

If the rotor turns at an angular velocity Ω, then the tangential centrifugal forces shown in Figure 3 act on the rotor blades.

Within the rotor blades, tensile loads dependent on the rotation velocity are dominant; ideally these would be canceled out where they affect the hub or tower head. Unavoidable divergences in the geometry and mass of the rotor blades, resulting from their

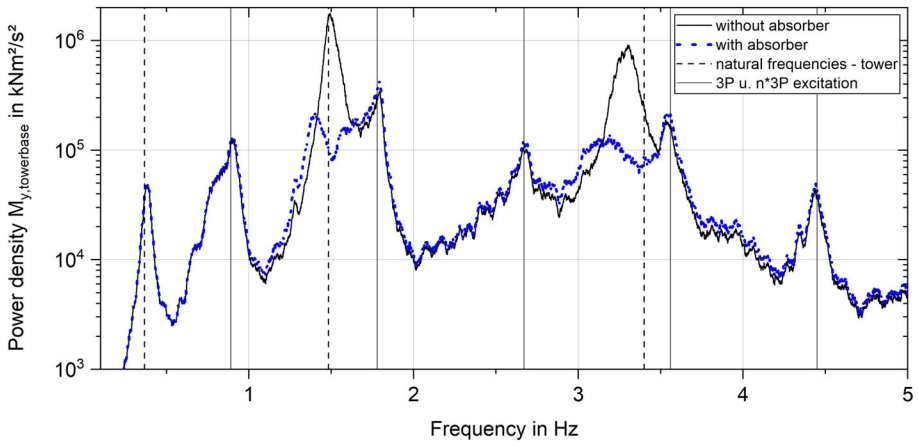

FIGURE 4 A rectangular time course of the normalized blade root moment (top) due to the tower shadow, leading to the excitation of higher harmonic frequencies; results from the associated Fourier analysis (bottom) at an average rotational speed of 18 rpm

manufacture, disrupt this equilibrium. The unbalanced mass in the rotor which results from this Reference 23 applies the relevant periodic differential force to the entire system. As there is no evidence of significant natural frequencies in the vertical direction, only horizontal excitation is considered important. This mainly leads to 1P excitation of the WT's lateral vibrations.

Besides the type of excitation arising from the rotating masses, we discuss below three further effects arising from the aerodynamic incident flow to the rotor blades and the tower. If we assume a mean wind speed, increasing with height, then on average the greatest flow forces apply to the rotor blades at the point where they point vertically upwards, and the lowest apply at the point where their tips point vertically downwards. This differential in forces means the center of pressure in a three-bladed turbine shifts upwards on the rotor plane, and the hub is exposed to 1P circumferential bending. Higher harmonics play less of a role here due to aerodynamic nonlinearity.

The most marked effect of the rotor loads arises through the aerodynamic interaction between blades and tower. The wind speed which is reduced locally due to the tower shadow effect causes a short-term, impulse-like dip in the aerodynamic blade forces when the blade passes in front of the tower. This impulse-like excitation arises with every cycle, that is, with $n \cdot \Omega$ (3P excitation), and is input into the tower structure via the drivetrain.

Figure 4 above shows developments over time in the moment of impetus at the blade root, calculated and normalized using a MBS. A rectangular impulse can clearly be seen to recur with each cycle. As the Fourier analysis confirms (bottom of Figure 4), higher harmonics ($f = n \cdot \Omega$) only subside a little and the whole system is excited to a non-negligible degree. The short-term dip in flow forces on the rotor blade is dependent on the distance from the hub, as shown on a diagram in Reference 15. In comparison, the effect of the mass imbalances presented in Figure 3 only lead to a dominant peak at $f = \Omega$.

Where there is no rotor movement in a WT, flow surrounds the cylindrical cross-section of the tower structure. The phenomenon of a Kármán vortex,[17] with which we are familiar from chimneys and other building elements with circular (hollow) profiles, can excite the load-bearing structure, causing vibrations. In order to determine the excitation frequency for a circular cylinder, a simplified Equation (1) applies with a Strouhal number of $St = 0.20$, an average wind speed v and a circle diameter d.[24] According to Reference 19, this phenomenon has not yet been observed in the WT's operating state, as the field of flow generated by the rotor disrupts the formation of a vortex. In numerical flow simulations performed by the IAG, vortices are visible even in the operating state, but these lose their dominance when compared to a stationary turbine.

$$f = 0.2\,v/d \tag{1}$$

The structural excitation effects show that both the 1P and 3P excitation are dominant, but also that their multiples bring significant vibrations into the WT system. This is presented in detail in References 15 and 19.

3.4 | Attenuation

Besides the exciting effects described above, the real oscillation amplitude in a WT is determined by various other effects. Structural attenuation in steel and reinforced concrete structures plays a secondary role. It could, for example, reach $\delta = 0.015$ (logarithmic decrement[17]) for steel chimneys, according to Reference 25.

Thus, with the WT observed for the present research, attenuation in the ground only caused a negligible reduction in amplitudes.

When a WT is operating, aerodynamic or aerodynamic force attenuation is dominant and directly dependent on the turbine's tip speed ratio λ[15] (in this case, $\lambda = 6$).

One way to depict this using a simplified model is as a viscous damper which influences the translational degree of freedom in the head of the tower.

A more precise observation also shows a tilting motion of the rotor to cause attenuating effects. Measurements of aerodynamic attenuation and step-by-step instructions are available in Reference 19. For the reference turbine simulated in the present study we assumed that, at a wind speed of 10 m/s, viscous attenuation would be 12 Ns/mm. A simulated test to show vibration dissipating gave a logarithmic decrement of $\delta = 0.1$. This value may rise in the nominal load range.

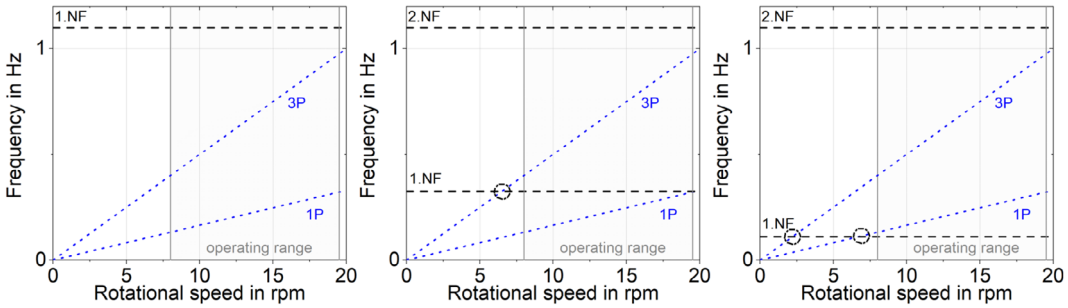

FIGURE 5 Modeling depth of the hybrid tower, beam and shell models, shell modes in the tubular steel tower

TABLE 1 Comparison of the natural frequencies in Hz assuming stiff foundation clamping

Type of vibration	Cantilever arm vibration after EC1-4	Estimate after *Morleigh*	Beam model in/across wind direction	Shell model	MBS
First TBEF	0.43	0.37	0.35/0.35	0.35	0.36
Second TBEF	–	–	1.45/1.46	1.46	1.52
Third TBEF	–	–	3.30/3.30	3.33	3.33
Fourth TBEF	–	–	6.17/6.19	6.22	6.69

4 | SIMULATION METHODS

4.1 | Depth of modeling and model design

If we are to capture the dynamics of a WT appropriately, we need to simulate the overall dynamics. Such simulations are not only used to optimize turbine control but are also needed to determine those loads at play on the tower that are relevant to measurements, as in Reference 18. This contrasts with a quasi-static measurement procedure. In these simulations, the individual loads affecting the turbine are normally simulated for the time interval using the design load cases (DLCs). The simulations consider the properties relevant to structural dynamics, such as the stiffness and mass distribution in all WT components (hub, rotors, gearbox, tower and foundations), the aerodynamic interaction with the turbulent incident flow, and the WT control system. We examine the best simulation method for this, MBS, in more detail in Section 4.5. However, a precise knowledge of the blade geometry and control system parameters is required in order to perform the simulations.

It is not possible to simply estimate the effects to be expected for a particular WT. If the intention is to capture only the major characteristics of the vibrations induced in the ground, one option is to apply a reduced model of the WT as a tower structure/head mass model (Figure 5). As we determine in Section 6 below, the frequency of blade passage as explained in Section 3.3 and its higher-harmonic multiples play a key role, which in turn means that the rotational velocity must be known in order to produce a simplified observation. This can be estimated for a given wind speed using the power coefficients and curves—which depend on the mean wind speed—and the outer limit values for the rotational speed range. For many types of turbine, the information required will be provided by the manufacturer.

The tower structure must reflect the geometric and material properties outlined in Figure 5. In addition to this, as part of our research we created a finite element model based on beam elements and a high-definition surface model based on shell elements. The shell model aims both to depict more precisely the variation in stiffness and mass distribution with height, and to identify any shell modes which contribute to sound radiation (on the right-hand side of Figure 5). The comparison in Table 1 of calculated natural frequencies shows divergences of < 2% between the two modeling approaches. For the purposes of quick pre-dimensioning, the approximation after *Morleigh*[17] with a divergence of ~ 6% is an efficient alternative tool, which considers both the variation in stiffness and mass distribution with tower height, and the head mass. In this particular case, the tower structure was divided into seven segments for these purposes (Index i).

The segment-dependent masses were raised on a horizontal cantilever arm as individual horizontal loads (F_i) and a deformation calculation was performed. Evaluation was performed taking account of acceleration due to gravity g, and horizontal deformations (u_i) of the mass points in accordance with Equation (2). Due to the large tower mass involved in the vibrations, the simplest estimate as a cantilever arm vibration with a single head mass, such as that in Reference 24. Annex *F*, diverges by 23% from the numerical solution.

$$f = \frac{\sqrt{g\frac{\sum(F_i \cdot u_i)}{\sum(F_i \cdot u_i^2)}}}{2\pi} \tag{2}$$

For the more precise numerical observation, a preferred direction for the natural modes should be identified. An example of this is shown in the "beam model" in Table 1. This direction arises from the

eccentricity of the head mass in relation to the center of gravity for the tower diameter, but only plays a minor role at low natural frequencies. Depending on the local conditions on the ground, natural frequencies may diverge from the upper limit value when a fully rigid foundation clamping system is applied. Small divergences can be observed in comparison to the MBS. Some of these can be traced back to interaction between the vibrations in the blades and in the tower, and some to the mass's second moment of area—which is not mapped in the lumped head mass.

The comparisons between simulation and measurement data discussed in Section 6.3 do not elicit any points of note within the frequency range observed which could be traced back to the excitation of shell modes. This shows that the significantly greater modeling and calculation effort for a shell model is not necessary for the ground vibrations observed in the present research. We therefore performed all subsequent research using the beam model. Several procedures are suitable for calculating the dynamic behavior. Unless otherwise stated, calculations have been made using Ansys v19.2.[26]

The present study does not explore the dynamic basis for oscillating systems. We recommend that readers who are interested look at the thorough presentation in Reference 17 or the summary of linear and non-linear vibration problems and the numerical treatment of these in References 27 and 28.

For all our calculations, we have assumed a linear vibration problem in the operating state. If this condition is not met, additional challenges arise in both the numerical solving of equations[29] and the interpretation of results.[30]

4.2 | Eigenvalue analysis

If a system capable of vibrating moves out of its resting state or is subjected to an impulse load, the dissipating vibration can be described using the homogeneous differential equation of motion. The frequency at which it settles corresponds to the relevant natural frequency, and the movement mode corresponds to the relevant natural mode. It is determined by solving an eigenvalue problem based on system matrices. Given the usual degree of attenuation for structures, the influence on the resulting natural frequency is negligible.

4.3 | Harmonic analysis

For a harmonic load, the homogeneous solution of the differential equation dissipates due to attenuation and the structure follows the pattern of load applied over time with a phase shift and modified amplitude. The amplitude ratio between excitation and response signals is described using the amplification function. In the simulation, this stationary state is reflected in a frequency response analysis or harmonic analysis. The calculation allows turbine builders to record the effects of harmonic excitations on other system components and is restricted to structures with linear geometric and material properties. When observing WTs, the basic idea of a steady state should not be disregarded. Some real excitations, such as the first tower natural frequency in operating state (see Section 7), do not normally affect this stationary state, but present as dominant due to the resonance in the simulation results. If these phenomena are evaluated appropriately, the calculation process will help to record the effects of structural changes quickly. Besides the amplitudes applied constantly over the whole frequency range under observation, the current finite element programs can also apply phase angles and other frequency-dependent loads, and thus account more precisely for the excitation characteristics.

In the context of the present research, the results prepared using a Fourier analysis were subjected to a MBS (Section 4.5) for our subsequent investigations.

4.4 | Transient analysis

Transient analysis calculates the movement equation for each time interval. We say that this equation is solved in the time domain. For the present research, these calculations were normally only performed when testing to show vibration dissipating or when assessing selected states. We performed the actual solution in the time domain using MBS.

4.5 | Multi-body simulation

MBS is a numerical simulation process not used as standard in construction. Multiple stiff or soft bodies are connected using kinematic constraints to form an overall model. This ensures their interactions can be calculated efficiently. The solution can either be in a linearized state, for example, to determine the natural frequencies of the overall system, or in the time domain using numerical integration processes. We used the Simpack MBS software[31] for the present research. The methods of analysis described in Sections 4.2-4.4 can be applied to this procedure.

The MBS topology for a horizontal axis WT comprises the basic components: foundations, tower, nacelle, drivetrain, hub and rotor blades. The tower, rotor blades and some components of the drivetrain are normally incorporated into the beam formulation as flexible bodies. With more complex building elements that have elasticities which cannot be disregarded in the analysis case, their structure is meshed in an external FE tool, modally reduced and incorporated into the MBS. Examples of these include the machine frame and the shell model for the tower. The system matrices transferred between programs contain mass and stiffness distributions, natural modes and natural frequencies. Time integration for the model as a whole is clearly accelerated in this case and the deformation of a body is described by superposing a limited number of natural modes.

When designing a WT and calculating the relevant turbine loads according to DLCs, it is sufficient to consider the natural frequencies of tower and rotor blades up to a limit of 20 Hz. However, should more complex phenomena be observed, such as the propagation of higher-frequency drive vibrations, higher natural frequencies must be activated accordingly. When partial models are being meshed,

the frequency range under observation should be taken into account.

The turbine model interacts aeroelastically with the turbulent incident flow. The distribution of wind speed over space and time is stochastic and can be described spectrally, for example, using the Kaimal spectrum.[32] An "inverse transform" builds the time signal for a 3D wind field which is subject to turbulence from this frequency spectrum. It can be compared to generating synthetic processes for paths of motion in the earth caused by earthquakes. The relative movements between the rotor blade profile and the local wind speed induce changeable flow forces over the rotor blade. These can be calculated using the blade element impulse method.[15]

5 | SEISMIC MEASUREMENTS

Seismic measuring stations, such as the Gräfenberg array in the Franconian Jura, are employed to identify earthquakes or to monitor the nuclear Non-Proliferation Treaty. In order to ensure measurements are valid, such measuring stations will ideally be located in places with few disruptive influences, for example, in the galleries of abandoned mines. With the increase in numbers of onshore WT in recent years, an increase in influences on these measurements has been observed. Discrete frequencies which can clearly be ascribed to WTs were identified when many sets of measurement data were evaluated.[33–35] These ground motion have been observed at distances of up to several kilometers away, and interpreted as a superposition of specific WT natural frequencies with the 3P excitation and its multiples.

For the research conducted in the context of the present study, broadband seismometers were installed along a profile at distances of up to ~1.8 km from the reference WT, as described in Section 2.1. In order to measure the WT as a source of vibrations, free from other disruptive influences wherever possible and without any additional changes while the waves were propagating, we aimed to achieve a strong coupling between a sensor and the WT. The seismometer was installed underground at a distance of around 3 m from the external wall of the tower, near the outer edge of the foundations. The layer of soil above the WT foundation can be neglected for the frequencies observed (<10 Hz). We ensured that the sensor was well connected to the ground when it was installed, in order to minimize any coupling effects. At a sampling rate of 100 Hz, the recording instruments detected very small seismic vibrations (<1 μm/s ground motion velocity), both in two horizontal directions (N-S and E-W) and vertically (Z). Time synchronization for the sensors was achieved using the GPS signal, and the specific influences of the measuring equipment on the measurement signal were eliminated by deconvoling the instrument response at a software level.

During the measurement campaign, the WT was intentionally switched off for 20 minutes every 2 hours. In this study we only account for the vertical ground vibrations measured by the sensor on the WT foundations, as this characterizes the source of vibration without any influence from propagation through the subsoil. Both the IBF and the GPI at the KIT are currently researching work for publication about azimuth-dependent effects on signal amplitudes with

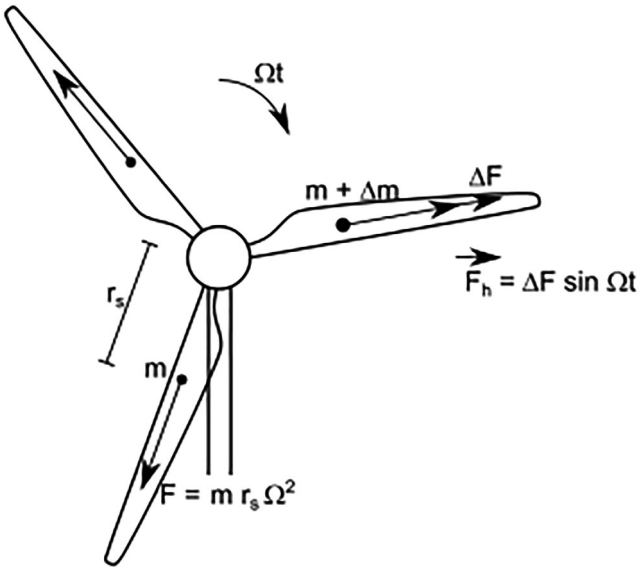

FIGURE 6 The frequency spectrum for the vertical ground vibration velocity at the seismic sensor on the foundation of the WT within a 3 hours time interval

regard to wind direction, wave propagation along the propagation path, the influence of the ground and stratification, and the near field and far field effects. Figure 6 shows the spectrogram for the ground motion velocity over a 3-hour period. Using the Fourier transform for overlapping time intervals of 20 seconds, the frequency components were calculated in the frequency range 0.1 to 30 Hz and are shown as a power spectral density over time. The colors reflect the intensity of power spectral density in dB relative to the spectrogram's maximum.

The period when the WT is switched off can be seen clearly in Figure 6 from $t = 100$ minutes. The time intervals marked on the spectrogram (Figure 6, red and blue) form the basis for calculating the mean power spectral density over a period of 10 minutes. Using the power density spectra, Section 6 illustrates and interprets the influence of the rotor motion through comparison with a non-rotating WT under the same wind conditions.

Wind measurements performed by the Wind Energy group of Stuttgart University at the same time, at a height of 10 m in the immediate surroundings of the WT (around 150 m away) with an extrapolation to hub height, gave a mean wind speed of 8 to 9 m/s. Combined with the estimate procedure set out in Section 4.1, this gives a rotational velocity of around 16 rpm: a sample operating state in the partially loaded range. In the research project described, additional operating states were studied both using measurements and numerical simulations. As the present paper outlines fundamental principles, we will not explore these findings in any further detail.

The power spectral densities of the ground vibrations measured during the present research are of an order of magnitude comparable to that of microseismicity at sea, but in a higher frequency range. It is not possible to make a direct statement on the propagation path, or any possibility of perceiving this, in the context of the results presented here.

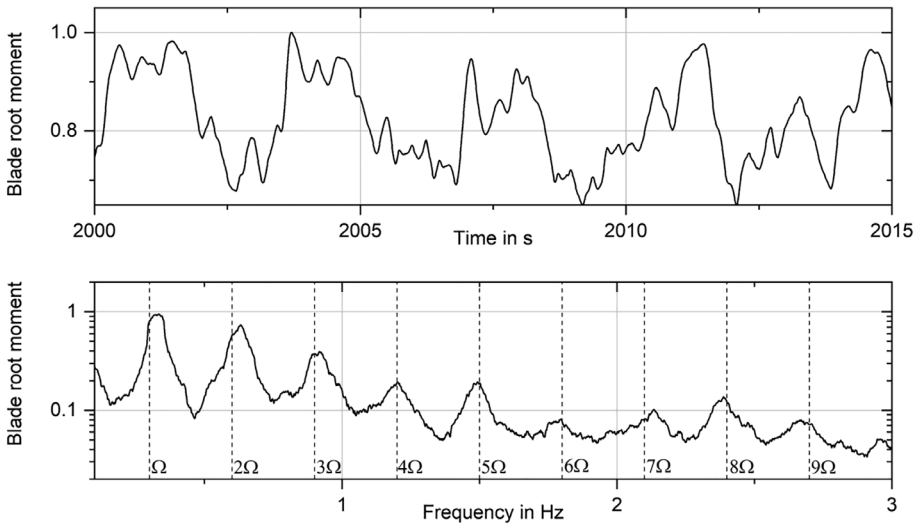

FIGURE 7 Variation over time of the vertical vibrations velocity measured at the outer edge of the foundation in the operating state (red) and with the turbine switched off (blue)

6 | DISCUSSION OF RESULTS

6.1 | Interpreting measurement data

The spectrogram presented in Figure 6 forms the starting point for our observations. The mean rotor thrust caused an average excursion in the WT head of 0.15 m under the applicable wind conditions. The head of the tower oscillated by ±0.13 m in the horizontal plane.

These values can grow to 0.2 m ± 0.2 m subject to a full load.

In the turbine's operating state, discrete frequencies with a high-power density can be identified across the entire frequency range. Some of these frequencies (such as 0.8, 1.6 or 2.4 Hz) vary little over time and arise at regular intervals as multiples of 0.8 Hz. Similar discrete frequency components have already been registered in the vicinity of WTs using other seismic sensors and can be correlated to the rotational velocity. We therefore assume that the frequency components we observed, which varied over time, were the 3P excitation and its multiples. The variation in frequencies measured can therefore be said to have been caused by a change in the turbine's rotational velocity. A further, very pronounced example of a signal for a variable frequency was identified in the 20 Hz range. This signal seemed to follow the turbine's rotational movement and was probably due to effects arising from the generator technology. Research is currently underway into the extent to which the measured signal is due to an electromagnetic input into the sensor or whether it is a true seismic vibration signal.

Besides these bands in Figure 6 which vary across frequencies, lines of increased power density also arise at constant frequency. Some of these frequency bands could also be identified when the turbine was switched off and must therefore have arisen from the natural frequencies of individual structural components in the WT. When considered across the entire frequency spectrum, significantly fewer vibrations were emitted into the ground when the turbine was switched off. Figure 7 compares the measured time signals in both operating and switched-off states, showing that the oscillation amplitudes right at the WT foundation differed by several orders of magnitude.

6.2 | Interpretation of vibration components

Next, we analyzed in details the time intervals marked in Figure 6 (in red and blue) as snapshots of the power spectral density (0.1-5 Hz). This frequency range is particularly relevant for investigating the tower structure on which we focused in our research. Figure 8 presents the mean power spectral densities of the vertical ground motion velocity for these two time intervals. Those phenomena derived from the simulation models that are attributable are depicted using vertical markings. The natural frequencies marked relate to the generic turbine. In this low-frequency range, the determining structural properties of actual and generic turbines are very similar, meaning that the frequency bands of the generic turbine form a sound basis for phenomenological mapping of the measured spectra.

With the turbine in an operating state, the 3P excitation and some of its multiples could be identified clearly. If these excitations were close to blade or tower natural frequencies, they amplified the amplitudes. The 3P excitation was so intense that it resulted in a significant system reaction, even where there was no natural frequency nearby. The highest power spectral density was induced in the ground in the range of the second TBEF (1.5 Hz), the next highest by the third TBEF (3.33 Hz) and then the 3P excitation (0.8 Hz). At this point the second multiple of 3P excitation matches a rotor blade natural frequency and the tower vibration.

When compared with the results in the time interval when the WT was switched off, the amplitudes which can be identified over time (Figure 7) are significantly lower and can also be seen in a semi-logarithmic representation. Some of the frequency peaks which arose when the WT was operating, especially close to the TBEFs (marked with an a), could also be identified when it was switched off.

Some frequency peaks in the operating state which could not be explained (marked with a b) also arose in a weaker form when the turbine was switched off. Other frequency peaks which were identified in the operating state (marked with a c) were overshadowed by other effects. The maximum ground excitation close to the second TBEF dropped away to a significantly lower level (marked with a d). It is

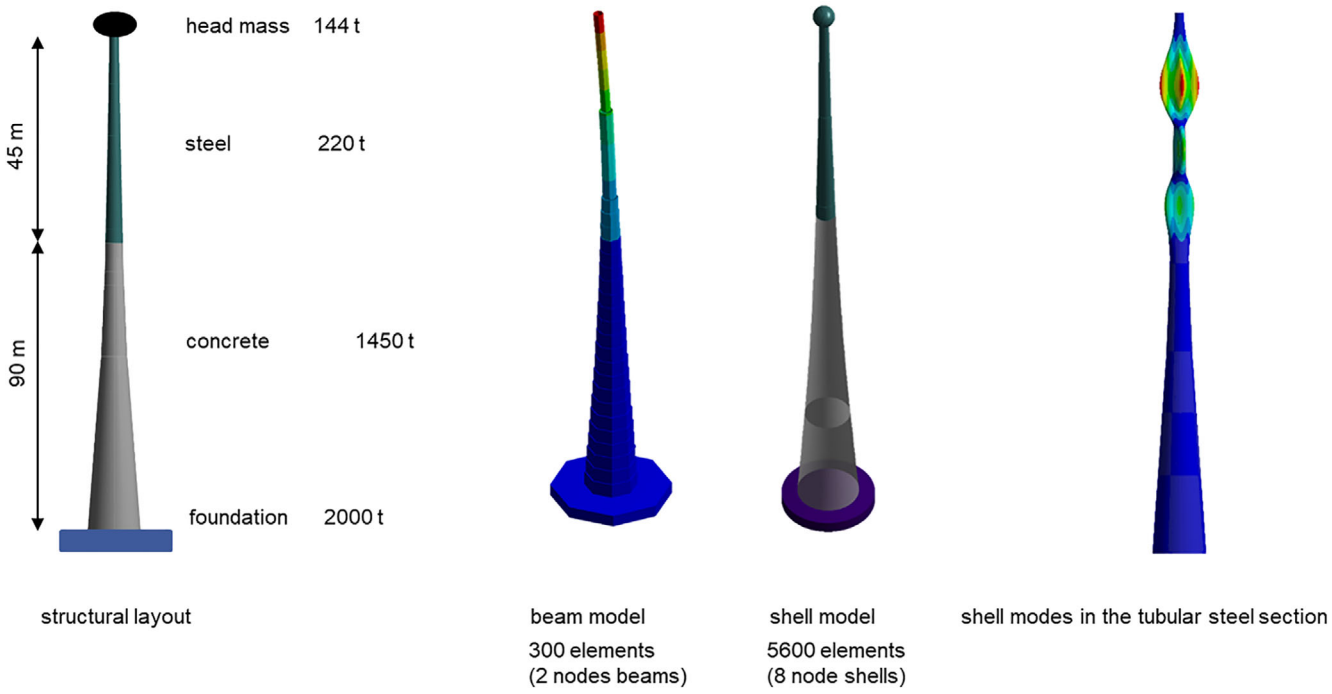

FIGURE 8 Comparison of the power spectral density for measurement 1 in the operating state (red) and when the turbine was switched off (blue); the colors correspond to the marked time windows in Figure 6. Markings a-e denote vibration phenomena which are explained in the text

striking that the first TBEF was at almost the same level here as in the operating state, and now dominated the vibration behavior (marked with an e). At the applicable wind speed of 8 to 9 m/s and with a tubular steel tower diameter of 2.1 to 4.2 m, Equation (1) shows that Kármán vortices may occur at a shedding frequency of 0.38 to 0.76 Hz. These vortices will thus lie very close to the first TBEF of 0.36 Hz and may explain the excitation when the turbine is switched off.

The aerodynamic attenuation described in Section 3.4 does not affect this state.

6.3 | Comparing measurements and simulation

In order to evaluate the simulation model, the measurements presented in Section 5 were compared with simulations in accordance with DLC 1.1 (normal operation as per IEC 61400-1[1]) for similar mean incident flow velocities. In Figure 9, the power density spectrum, averaged over the time interval, for seismic measurements of the rotating WT (Figure 6, red) is compared with the results of an MBS. Both the simulated and the measured progressions have been scaled to their respective maximum values. This was necessary because, for the simulation results, the restraining moment at the foot of the tower or the square of its change over time is considered to be an equivalent variable (vibrations M_y in and M_x across the wind direction).

In general, a correlation can be identified between the simulation and the measurement, both in terms of the amplitude ratio and in terms of the frequency of the peaks which arise. The effects described in Section 6.2, such as 3P excitation and its multiples or the dominance of the second and third TBEFs, are reflected in the numerical model. However, some individual effects which have not been explained (marked with an a) arise either in the simulation or in the measurements, but none is reflected in both. By way of an example, the dominance of the second and third TBEFs can be explained using the modeling. Four key mechanisms interact:

1. Excitation close to the natural frequency leads to resonance phenomena and major amplitude responses, even in an attenuated system.
2. Instinctively, the first natural bending frequency would perhaps be ascribed to the largest mass involved in vibration, due to the size of the head mass. However, calculation of modal masses (as a byproduct of eigenvalue analysis)[36] shows that more masses are involved with the second TBEF (Figure 10). This can be explained by the hybrid construction of the tower and would not be expected to occur with a purely tubular steel tower. The greatest displacements with the first natural bending mode occur at the head of the tower. This is where a head mass of some 150 t sits atop a relatively light tubular steel tower (~220 t).
   With the second natural bending mode, the excursion of the head is significantly lower and the maximum excursion lies in the area of the tower where the tubular steel and concrete meet. Hence a significantly larger proportion of the concrete structure is involved in this vibration mode.
3. A determining factor in the vibrations observed is the tilting motion of the elastically embedded foundations. As can be seen in

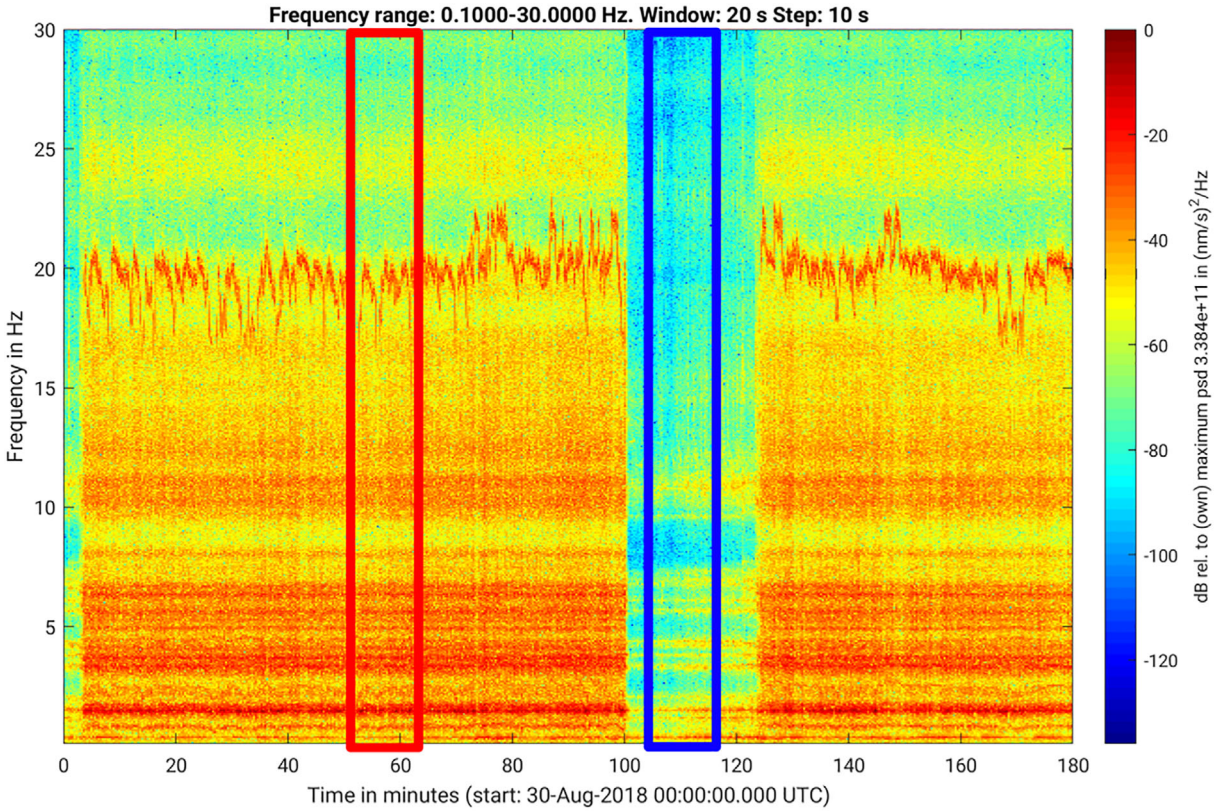

FIGURE 9 Comparison of the normalized power spectral density of the rotating WT (red) and the multi-body simulation (green)

FIGURE 10 Tower natural modes including foundation tilting and associated modal masses

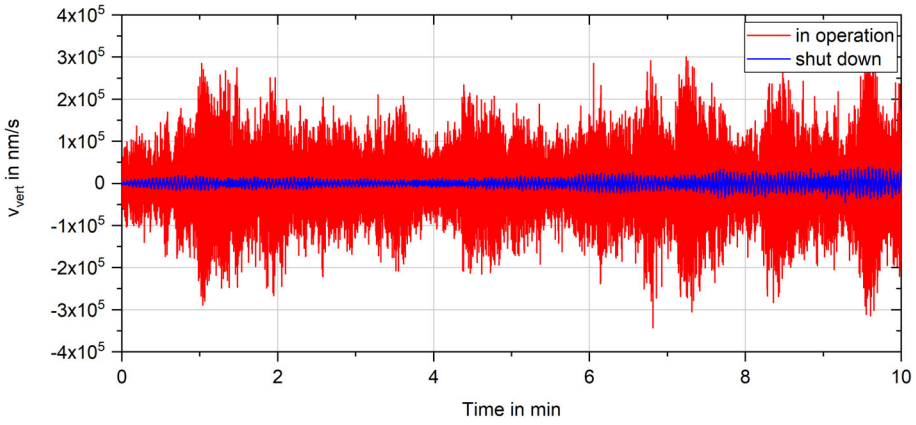

Figure 10, local curvature in the elastic line increases as the number of bending half cycles increases. This local curvature indicates the restraining moment and correlates directly to movement of the foundations.

4. Compared to the first natural bending mode, the horizontal movements of the tower head in the wind direction are much lower with the second natural bending frequency. Thus the first TBEF is attenuated to a much greater extent by the aerodynamic damping arising from the horizontal movement.

Hence deviations between the simulation and measurement results can arise for a variety of reasons. First, the simulation model cannot access the original WT data, but only the generic model described in Section 2.1. The simulated incident flow conditions used here were measurement scenarios and assumed statistical turbulence models which diverge from the real conditions. The position of the seismometer could not be adjusted to reflect the changing wind direction. This meant it was not possible to categorize the vibration directions clearly as "in" or "across" the wind direction or,

TABLE 2 Details of the absorber design

Name	Natural mode/ frequency in Hz	Modal mass in t	z position in m	Absorber mass in t	Stiffness in N/mm	Damping in Ns/mm	Natural frequency of absorber element in Hz
Absorber 1	Second TBEF/1.52	457	93.7	9.14	801	13.4	1.49
Absorber 2.1	Third TBEF/3.33	245	111	2.45	1051	6.12	3.30
Absorber 2.2	Third TBEF/3.33	245	65.5	2.45	1051	6.12	3.30

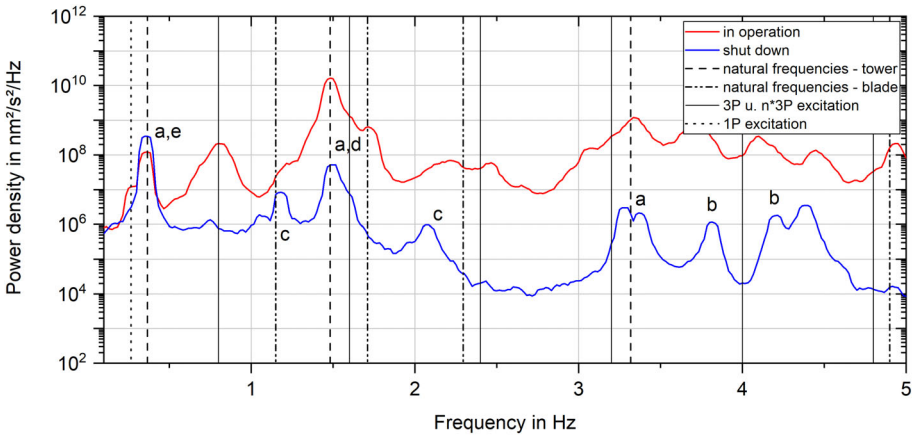

FIGURE 11 Normalized natural modes of the second and third natural frequency with absorber position

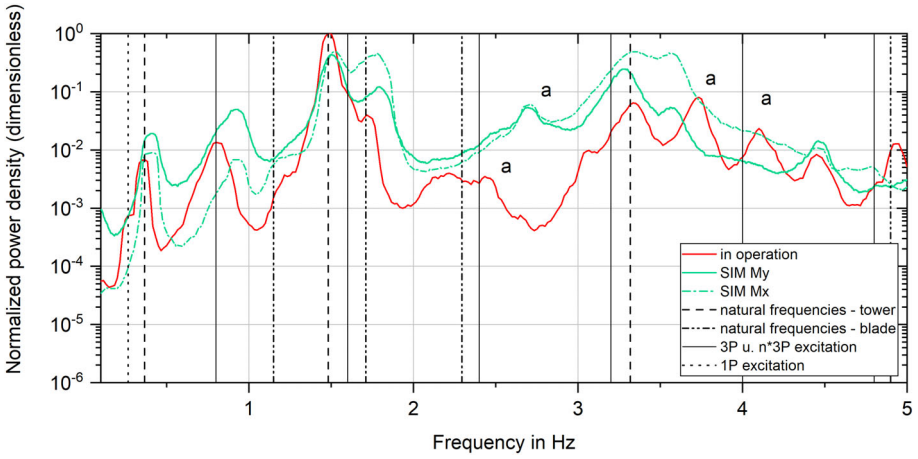

FIGURE 12 Effects of the absorbers on the power density spectrum of the vertical movement at the foundation's outer edge in the steady state

therefore, to compare these directly with the simulated values. Second, deviations are inherent in modeling. However, it is clear from the model that vibrations induced in the ground and the underlying vibration phenomena depicted using the simulation model can be explained and influenced by turbine parameters.

7 | REDUCTION USING A VIBRATION ABSORBER

Slender skyscrapers such as Taipei 101 and lightweight pedestrian bridges, chimneys and stairways normally use vibration absorbers. The basic principles for reducing natural frequency oscillation in a system susceptible to vibration using suspension and damping elements to connect a mass were developed theoretically by Den Hartog as early as 1937 and made accessible for construction applications in Reference 17.

The theoretical calculation approaches can only be directly applied to systems with no damping or weak damping. The aerodynamic attenuation described in Section 3.4 and the particularities of WTs described above give us cause to investigate the effect of absorbers. As discussed in Section 6, the second and third natural bending modes of the WT tower observed dominate the vibrations induced in the ground. The power density of these two TBEFs should be reduced. To that end, each of these types of vibration must be

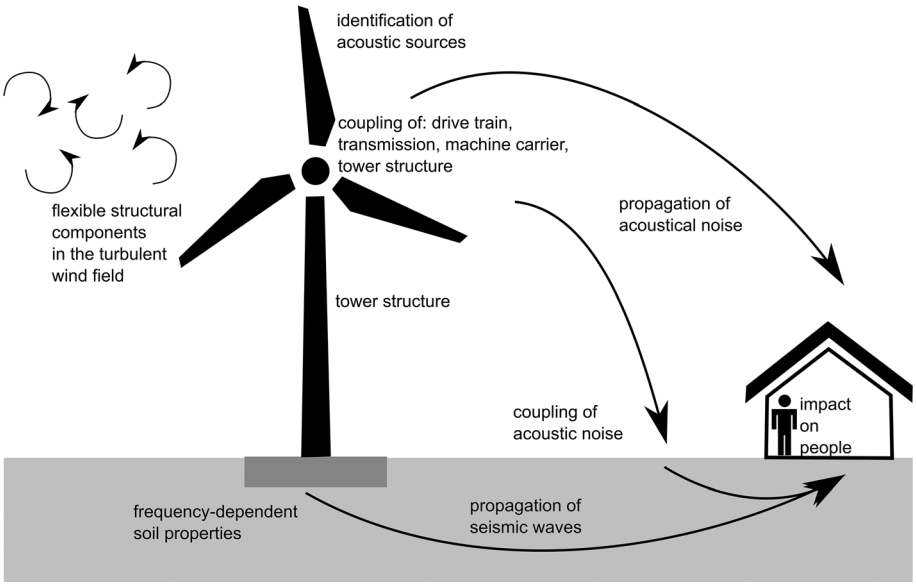

FIGURE 13 Reduction of spectral power density input from the tower's second and third natural frequencies through the use of absorbers; evaluating the spectral power density of the tower base moment using a MBS in the time domain

investigated individually and the dynamic properties of the allotted absorber elements determined. The parameters shown in Table 2 should be applied to the generic reference turbine.

As shown in Figure 11, the absorber is positioned at the local extremity of the bending curve for the relevant type of vibration. To simplify, the effects in the harmonic analysis shown in Figure 12 were investigated given both the aerodynamic damping and the foundations' elastic support and viscous attenuation.

An assessment was made of power density at an observation point on the outer edge of the foundations, behind the tower structure in the direction of incident flow. The frequency-dependent amplitude of force excitation results from the MBSs and is only pronounced in the incident flow direction at the tower head. The values correspond to the operating state described in Section 5 at wind speeds of 8 m/s.

Unrealistic amplitudes appear in the results close to the first natural bending mode.

It is particularly important to assess these, as they bear no commonalities with the behavior subject to real excitation.

In both sets of load circumstances, comparing structures with and without absorbers, an optimized absorber distribution reduces power spectral density by a factor of between 250 and 600. It is not possible to transfer these values directly; this can only be quantified using the MBSs depicted in Figure 13. Subject to the real excitation with variable rotational speeds observed in these, and with an associated non-harmonic influence, decrease in the power spectral density induced in the soil reduces by a factor of 10.

To summarize, we have established that vibration absorbers represent a suitable means of reducing the vibrations which the WT induces in the ground. They can be used selectively to positively influence individual vibration phenomena and the associated frequency ranges, in other words to reduce them.

The aerodynamic attenuation which appears in the present sample calculations does not significantly influence the process of eradicating these vibration phenomena.

8 | CONCLUSION

In the research we have presented here, the results of simulations and measurements of vibrations emitted by a 2 MW WT have been compared. Our aim has been to investigate the technical circumstances at the turbine and thereby describe the source of potential emissions. In so doing we have observed the power density of vibration emissions arising at the foundations of the turbine, both while it is operating and while it is not. We identified and explained effects of both the rotor motion and the structural properties of the tower's load-bearing structure, and we proposed measures to reduce the vibrations induced in the ground.

Employing vibration absorbers means the oscillation amplitude arising at discrete frequencies can be reduced. Please note that the results presented as part of the present paper do not permit us to draw direct conclusions about far field impact, as we have not considered the propagation mechanisms.

ACKNOWLEDGMENTS

The authors would like to thank the Federal German Ministry for Economic Affairs and Energy for supporting the research presented here, and all their project partners for their good, fruitful cooperation.

REFERENCES

1. IEC 61400-1 (2005) Wind turbines—Part 1: Design requirements. August 2005 issue.
2. Seidel M. Zur Bemessung geschraubter Ringflansch- verbindungen von Windenergieanlagen [unpublished dissertation]. Hannover, Germany: Leibniz Universität Hannover; 2001.
3. Schaumann P, Steppeler S. Ermüdungsverhalten von Schweißverbindungen von Tragstrukturen für Windenergieanlagen bei sehr hohen Lastwechselzahlen. Schweißen im Schiffbau und Ingenieurbau, DVS-Berichte 277. Düsseldorf, Germany: DVS Media, 2011; p. 53–58.
4. Jay A, Meyrs AT, Torabian S, et al. Spirally welded steel wind towers: Buckling experiments, analyses, and research needs. J Constr Steel Res. 2019;125:218–226.

5. Weidner P, Mehdianpour M, Ummenhofer T. Ermüdungsfestigkeit einseitig geschweißter Stumpfstöße von Kreishohlprofilen. Stahlbau. 2016;85(9):620–629.
6. WindForS—Windenergie Forschungscluster: Forschungsvorhaben: TremAc; Objektive Kriterien zu Erschütterungs- und Schallemissionen durch Windenergieanlagen im Bin- nenland [online], 2019 [accessed 2019 Feb 12]. Available from https://www.windfors.de/de/projekte/tremac/
7. Kudella P. Objektive Kriterien zu Erschütterungs- und Schallemissionen durch Windenergieanlagen im Bin- nenland—das Verbundprojekt TremAc. In: Kötter Consulting Engineers [Hrsg.] 10. Rheiner Windenergie-Forum; 2019.
8. Gortsas TV, Triantafyllidis T, Kudella P, Zieger T. Low-frequency micro-seismic radiation by wind turbines and it's interaction with acoustic noise emission. 7th International Conference on Wind Turbine Noise, Rotterdam; 2017.
9. Klein L, Gude J, Wenz F, Lutz T, Kräme E. Advanced computational fluid dynamics (CFD)—Multi-body simulation (MBS) coupling to assess low-frequency emissions from wind turbines. Wind Energy Sci. 2018; 3:713–728.
10. Seidel M. Auslegung von Hybridtürmen für Windenergieanlagen: Lastermittlung und Nachweis der Ermüdungsfestigkeit am Beispiel einer 3,6-MW-WEA mit 100 m Rotordurchmesser. Beton- und Stahlbetonbau. 2002;97(11):564–575.
11. Bundesnetzagentur [Hrsg.] Anlagenregister [online]. [As at: July 2016]. https://www.bundesnetzagentur.de/DE/Sachgebiete/ElektrizitaetundGas/Unternehmen_Institutionen/ErneuerbareEnergien/Anlagenregister/Anlagenregister_node.html
12. Siemens AG, editor. Datasheet: Bolted steel shell tower. SIEMENS [online]. [accessed 2019 Mar 7]. https://www.energy.siemens.com/us/pool/hq/power-generation/renewables/wind-power/Bolted_Steel_Shell_Tower_brochure_EN.pdf
13. Bortolotti P, Bottasso CL, Croce A. Combined preliminary-detailed design of wind turbines. Wind Energy Sci. 2016;1(1):71–88.
14. Triantafyllidis T, Prange B, Vrettos C. Circular and rectangular foundations on halfspace: Numerical values of dynamic stiffness functions. In: Cakmak AS, editor. Ground motion and engineering seismology. Developments in geotechnical engineering. Volume 44. Amsterdam: Elsevier, 1987; p. 409–426.
15. Hau E. Windkraftanlagen: Grundlagen, Technik, Einsatz, Wirtschaftlichkeit. Berlin: Springer Vieweg, 2014.
16. Lange H, Elberg C. Entwicklung von weichen Tür- men für Windenergieanlagen—Softtower. Stahlbau. 2017;86(4):351–356.
17. Petersen C. Dynamik der Baukonstruktionen. Wiesbaden: Vieweg +Teubner Verlag, 2000.
18. Schriften des Deutschen Instituts für Bautechnik. Richtlinie für Windenergieanlagen—Einwirkungen und Standsicherheitsnachweise für Turm und Gründung. Series B, Volume. 8th ed. Oct; 2012.
19. Gasch R, Twele J, Bade P, et al. Wind- kraftanlagen; Grundlagen, Entwurf, Planung und Betrieb. Wiesbaden: Springer Vieweg, 2016.
20. Lukas P, Kunz L. Specific features of high-cycle and ultra-high-cycle fatigue. Fatigue Fract Eng Mater Struct. 2002;25(8–9):747–753.
21. Pyttel B, Schwerdt D, Berger C. Very high cycle fatigue—Is there a fatigue limit? Int J Fatigue. 2011;33(1):49–58.
22. Trško L, Bokuvka O, Nový F, Guagliano M. Effect of severe shot peening on ultra-high-cycle fatigue of a low-alloy steel. Mater Des. 2014;57:103–113.
23. DIN ISO 21940-1 (2018) Mechanische Schwingungen—Auswuchten von Rotoren—Teil 1: Einführung. Berlin: Beuth. Draft. May, 2018.
24. DIN EN 1991-1-4 Einwirkungen auf Tragwerke—Teil 1-4: Allgemeine Einwirkungen—Windlasten. Berlin: Beuth. Dec, 2010.
25. DIN 4133. Freistehende Schornsteine aus Stahl (withdrawn); Nov 1991.
26. ANSYS Inc, editor. Ansys Workbench v.19.2 [online]. [accessed 2019 Feb 21]. https://www.ansys.com
27. Nagel S. Studies on the seismic design of network arch road bridges [Masterarbeit]. Versuchsanstalt für Stahl, Holz und Steine, Karlsruher Institut für Technologie; 2015
28. Nasdala L. FEM-Formelsammlung Statik und Dyna- mik: Hintergrundinformationen, Tipps und Tricks. Wiesbaden: Springer Vieweg, 2015.
29. Simo J, Tarnow N. The discrete energy-momentum method. Conserving algorithms for nonlinear elastodynamics. Z Angew Math Phys. 1992;43(5):757–792.
30. Hagedorn P. Nichtlineare Schwingungen. Wiesbaden: Akad. Verl.-Ges, 1978.
31. SIMULIA, editor. SIMPACK—Multi-Body Simulation Software [Software]. [accessed 2019 Feb 26]. http://www. simpack.com
32. Kaimal JC, Wyngaard JC, Izumi Y, Coté OR. Spectral characteristics of surface-layer turbulence. Quart J R Meteorol Soc. 1972;98(417): 563–589.
33. Stammler K, Ceranna L. Influence of wind turbines on seismic records of the Gräfenberg Array. Seismol Res Lett. 2016;87(5):1075–1081.
34. Styles P, England R, Stimpson IG, et al. Micro-seismic and infrasound monitoring of low frequency noise and vibrations from wind-farms: Recommendations on the siting of windfarms in the vicinity of Eskdalemuir, Scotland. Keele, UK: Keele University, 2005.
35. Zieger T, Ritter JRR. Influence of wind turbines on seismic stations in the Upper Rhine Graben, SW Germany. J Seismol. 2018;22:105–122.
36. Ummenhofer T, Knödel P. Modal superposition according to EC8. Stahlbau. 2017;86(8):736–740.

How to cite this article: Nagel S, Zieger T, Luhmann B, Knödel P, Ritter J, Ummenhofer T. Ground motions induced by wind turbines. Civil Engineering Design. 2021;3:73–86. https://doi.org/10.1002/cend.202100015